

# Determining the escape fraction of ionizing photons during reionization with the GRB derived star-formation rate

J.S.B. Wyithe<sup>1</sup>, A.M. Hopkins<sup>2</sup>, M.D. Kistler<sup>3,4</sup>, H. Yüksel<sup>5</sup>, J.F. Beacom<sup>3,4,6</sup>

<sup>1</sup>*School of Physics, University of Melbourne, Parkville, Victoria, Australia*

<sup>2</sup>*Anglo-Australian Observatory, P.O. Box 296, Epping, NSW 1710, Australia*

<sup>3</sup>*Center for Cosmology and Astro-Particle Physics, The Ohio State University, 191 W. Woodruff Ave., Columbus, OH 43210*

<sup>4</sup>*Dept. of Physics, The Ohio State University, 191 W. Woodruff Ave., Columbus, OH 43210*

<sup>5</sup>*Bartol Research Institute and Department of Physics and Astronomy, University of Delaware, Newark, Delaware 19716*

<sup>6</sup>*Dept. of Astronomy, The Ohio State University, 140 W. 18th Ave., Columbus, OH 43210*

*email: swyithe@unimelb.edu.au*

Draft Version

## ABSTRACT

The fraction of ionizing photons that escape their host galaxies and so are able to ionize hydrogen in the inter-galactic medium (IGM) is a critical parameter in analyses of the reionization era and early galaxy formation. Studies of the reionization history normally suffer from a degeneracy between the unknown values for the efficiency with which high redshift galaxies turn mass into stars and the escape fraction of ionizing photons. Recent gamma-ray burst (GRB) measurements of the star formation rate density during reionization provide the first opportunity to break this degeneracy. We confront a semi-analytic model for reionization with the GRB-derived star formation rate, as well as observations of the Ly $\alpha$  forest and the CMB. Assuming that UV photons produced in star-forming galaxies dominate the reionization process, we show that the escape fraction of ionizing photons from high redshift galaxies is  $\sim 5\%$  [ $\log f_{\text{esc}} = -1.35 \pm 0.15$  (68%)] for our fiducial model. This value is reasonably stable against uncertainties in the modeling, including the implementation of radiative feedback, the possibility of an evolving escape fraction, and the unknown shape of the IMF, which in sum contribute  $\sim 0.2$  dex of additional systematic uncertainty on the value of escape fraction.

**Key words:** cosmology: diffuse radiation, large scale structure, theory – galaxies: high redshift, inter-galactic medium

## 1 INTRODUCTION

Star-bursting galaxies and quasars have been the leading candidates for the sources of the UV radiation required to reionize the hydrogen gas in the inter-galactic medium (IGM) (e.g., Barkana & Loeb 2001). The quasar population is observed to decline quickly at  $z \gtrsim 2.5$  and so it is believed that it was galaxies that contributed the bulk of UV photons that drove reionization (Madau et al. 1999; Fan et al. 2002; Srbainovsky & Wyithe 2007; Bolton & Haehnelt 2007). However, it has been difficult to make a positive case for galaxies as opposed to favoring them by disfavoring the case for quasars. The contribution of galaxies to the UV radiation field is dependent on the star formation rate and initial stellar mass function, but is also limited by the fraction of

ionizing photons that escape their host galaxies. If the escape fraction is small, then star formation had to be very efficient at high redshift in order to reionize the Universe. The escape fraction is therefore a critical parameter in studies of the connection between high redshift galaxy formation and reionization.

Attempts to determine the escape fraction have been dominated by direct observations of relatively low redshift galaxies, and by numerical simulation. Direct measurements of the escape fraction ( $f_{\text{esc}}$ ) are complicated by the fact that the intrinsic number of ionizing photons produced by a specific galaxy is unknown. A commonly adopted strategy to circumvent this limitation is to compare the flux observed at the Lyman limit to the observed flux at a frequency where the intrinsic emissivity can be inferred (Leitherer et al. 1995; Heckman et al. 2001; Deharveng et al. 2001; Steidel et al. 2001; Siana et al. 2007). The escape fraction at the Lyman limit can be then be derived using a model description of the

star formation history (Leitherer et al. 1995; Steidel et al. 2001; Siana et al. 2007). However the results are currently uncertain. At redshifts  $z \sim 1 - 3$ , observations have suggested a broader range of values for  $f_{\text{esc}}$ , from a few percent to  $\sim 20\%$  (Steidel et al. 2001; Fernández-Soto et al. 2003; Shapley et al. 2006; Siana et al. 2007). Inoue et al. (2006) have examined the evolution of the escape fraction in the redshift range  $z = 0 - 6$  using both direct observations of the escape fraction and values that they derive from measurements of the ionizing background. They find that the escape fraction evolves from  $f_{\text{esc}} \sim 1 - 10\%$ , increasing towards high redshift. More recently Fynbo et al. (2009) have used spectroscopic observations of individual GRB afterglows at  $z > 2$  to place a 95% confidence upper limit of 7.5% on the escape fraction for ionizing photons on the sightlines of these GRBs.

Theoretical modeling has concentrated on the absorption of ionizing photons as they propagate through the interstellar medium towards the IGM. Here also the results are not yet conclusive. For example, Wood & Loeb (2000) found  $f_{\text{esc}} \lesssim 1\%$  at  $z \sim 10$  suggesting that the escape fraction decreases towards high redshift due to the increased density of galactic disks. More recently, Razoumov & Sommer-Larsen (2006) used galaxy formation simulations incorporating high-resolution 3-D radiative transfer to show that the escape fraction evolves from  $f_{\text{esc}} \sim 1 - 2\%$  at  $z = 2.39$  to  $f_{\text{esc}} \sim 6 - 10\%$  at  $z = 3.6$ . In agreement with Fujita et al. (2003), Razoumov & Sommer-Larsen (2006) find that increased supernova feedback at higher redshift expels gas from the vicinity of star-bursting regions, creating tunnels in the galaxy through which ionizing photons can escape into the IGM. They also find that star formation may occur at slightly lower densities at higher redshift, which further contributes to the increased  $f_{\text{esc}}$  towards higher redshift.

Recently, detailed numerical simulations (Gnedin et al. 2007) have been presented that predict a value for  $f_{\text{esc}}$  between 1 and 3%, for halos of mass  $M \gtrsim 5 \times 10^{10} M_{\odot}$ , over the redshift range  $3 < z < 9$ . This very low efficiency of reionization would have profound effects on the reionization history. In addition to a small escape fraction in massive galaxies, Gnedin et al. (2007) further predict that halos with  $M \lesssim 5 \times 10^{10} M_{\odot}$  have an escape fraction that is negligibly small. We point the interested reader to Srinovskiy & Wyithe (2008) and to the review by Ciardi & Ferrara (2005) for a more detailed discussion of prior work on estimating the escape fraction.

A less direct avenue to determining the escape fraction is through modeling of the ionizing background at the end of reionization. Models of the reionization of hydrogen and the subsequent Ly $\alpha$  forest are subject to a degeneracy between the star formation efficiency of gas accreted into galaxies and the fraction of ionizing photons that escape the dense gaseous environment of the galaxy to ionize the IGM. In order to break this degeneracy, the true cosmic star formation rate must be known. For example, the escape fraction has been estimated at high redshifts by combining the ionization rate in the IGM with an estimate of the star formation rate obtained from measurements of the galaxy luminosity function (e.g., Bolton & Haehnelt 2007; Srinovskiy & Wyithe 2008; Faucher-Giguère et al. 2008). Assuming that the mean-free-path is accurately estimated, the escape fraction follows from comparison of the total

number of photons produced with the number that are ionizing the IGM. The primary drawback of this technique is that the observed luminosity functions are subject to uncertain corrections for extinction in galaxies, as well as a flux limit. The latter fact means that an extrapolation to lower galaxy luminosities must be performed in order to obtain a total star formation rate.

GRBs are now beginning to probe the star formation rate density in the era during which the Universe is thought to have become reionized (Salvaterra et al. 2009; Tanvir et al. 2009). In this paper we employ the recent determination of the star formation rate density (Kistler et al. 2009) out to  $z \sim 8.5$  based on a compilation of high redshift GRBs. As described below, this measurement of the cosmic star formation rate with GRBs is not subject to the usual large corrections required for extinction and unseen faint galaxies. By modeling the reionization of hydrogen we determine the star formation efficiency and escape fraction that is required to simultaneously reproduce the optical depth to electron scattering of CMB photons, the star formation rate density during the reionization era, and the ionizing background at the end of reionization. Inclusion of the star formation rate density as a constraint allows the star formation efficiency and escape fraction to be separately determined.

Our analysis is similar to that of Choudhury & Ferrara (2005, 2006), who modeled the reionization history and compared model predictions to a range of observables, including the star formation rate, the ionization rate from the Ly $\alpha$  forest and the optical depth to electron scattering of CMB photons, as well as the evolution of Lyman limit systems and the temperature of the IGM among others. However, here we limit our attention to the first three of these observables that most directly relate to determination of the escape fraction, and which can be most reliably predicted by an analytic model. Most importantly, we make use of the recent determination of star formation rate density from GRBs, which for the first time provide a measurement of the total star formation deep into the reionization era. We also quantify the statistical and systematic uncertainties on the model parameters.

The paper is organized as follows. In § 2 we discuss the determination of star formation rate density from high redshift GRBs, and review a simple estimate of the ionizing photon budget for reionization. We then describe other observational constraints (§ 3), as well as our semi-analytic model for reionization (§ 4). The resulting limits on the possible values of model parameters presented in § 5. We conclude with a summary of our results for the escape fraction in § 6. In our numerical examples, we adopt the standard set of cosmological parameters (Komatsu et al. 2009), with values of  $\Omega_b = 0.04$ ,  $\Omega_m = 0.24$  and  $\Omega_{\Lambda} = 0.76$  for the matter, baryon, and dark energy fractional density respectively,  $h = 0.73$ , for the dimensionless Hubble constant, and  $\sigma_8 = 0.81$  for the variance of the linear density field within regions of radius  $8h^{-1}\text{Mpc}$ .

## 2 A GRB DETERMINATION OF THE STAR FORMATION RATE DENSITY AT HIGH REDSHIFT

Kistler et al. (2009) (following Yüksel et al. 2008) have used

the counts of GRBs at high redshift to infer the star formation rate density out to  $z \sim 8.5$ . Inspection of their Figure 4 (see also Figure 1 of this paper) suggests that the star-formation rate density is as large as or could even be higher at  $z \sim 8$  than at  $z \sim 4 - 6$ , implying that the ionizing photon emissivity is not falling as observations move into the reionization era. This inference requires an assumption for the initial mass function. However since both ionizing photons and GRBs are produced by massive stars, estimates of the ionizing photon emissivity from the GRB rate should be fairly robust against uncertainties in the initial mass function (this point is taken up quantitatively in § 5.5). Kistler et al. (2009) argued that we have observed enough star formation via high redshift GRBs at  $z \gtrsim 6$  to reionize the universe. This conclusion was reached via a simple estimate of the number of ionizing photons produced prior to  $z \sim 6$  given the observed star formation rate density. For a Salpeter initial mass function, 4648 ionizing photons are produced per baryon incorporated into stars (§ 5.5). Taking this value, together with a constant star formation rate density for a time interval  $\Delta t$  the number of photons produced by stars per baryon of IGM is

$$\mathcal{N}_\gamma \sim 4 \left( \frac{f_{\text{esc}}}{0.1} \right) \left( \frac{\dot{\rho}_\star}{0.1 M_\odot \text{Mpc}^{-3}} \right) \left( \frac{\Delta t}{400 \text{Myr}} \right) \quad (1)$$

(Kistler et al. 2009). The inferred star formation rate density at  $z > 6$  implies  $\mathcal{N}_\gamma \sim 4_{-2}^{+4} (f_{\text{esc}}/0.1)$ . This is consistent with the modeling of Wyithe & Cen (2007) who found  $\mathcal{N}_\gamma \sim 4$  for reionization concluding at  $z = 6$  under a range of assumptions for the redshift range and efficiency of Population-III star formation, provided that the escape fraction of ionizing radiation is of order 10%. Thus, calculations based on the GRB-derived star formation rate density imply that there was sufficient star formation to complete reionization even with a relatively small value of  $f_{\text{esc}}$ .

In this paper we extend the simple estimates presented in Kistler et al. (2009). Specifically, we constrain the possible values of escape fraction by modeling the reionization history and comparing with the observed star formation rate density as traced by high redshift GRBs, the ionization rate as traced by the Ly- $\alpha$  forest at  $z < 6$ , and the optical depth to Thomson scattering of CMB photons. The GRB-derived star formation rate density values that were presented in Kistler et al. (2009) are special in three ways with respect to breaking the degeneracy between escape fraction and star formation efficiency during the reionization era.

Firstly, the star formation rate density is based on number counts of GRBs which yields the absolute death/birth rate of massive stars. These number counts are independent of the escape fraction that can influence other star formation rate indicators based on UV emission. The utility of counting events marking the death of individual stars in order to get the star formation rate density has also been argued by Lien & Fields (2009) in the context of supernovae at lower redshift.

Secondly, GRBs are thought to sample the full luminosity range of galaxies, so that no correction for luminosity function is required. In conventional studies of the star formation rate, one attempts to correct for both problems, but there are uncertainties (e.g., Hopkins & Beacom 2006). The GRB results from Kistler et al. (2009) confirm the two large corrections (for obscuration and luminosity function)

applied to the raw results of Bouwens et al. (2008). It could therefore be argued that this agreement implies the combined corrections are approximately correct, suggesting the absence of any deep misunderstandings about the properties of high redshift galaxies. Conversely, if the luminosity function correction applied to the Bouwens et al. (2008) data by Kistler et al. (2009) is appropriate, then most of the total star formation during the reionization era was within small galaxies. With regard to this point it is important to note that in more local samples, most GRB hosts are found to be low mass galaxies (Fruchter et al. 2006; Stanek et al. 2006). This implies that GRBs are an efficient probe of low mass galaxy formation, and is in contrast to studies of the UV luminosity function at  $z > 6$  that currently probe only the most massive galaxies. Since low mass galaxies seem to be dominant during the reionization era we therefore argue that GRBs provide the most important constraints on the star formation rate density during reionization, and utilize the star formation values from Kistler et al. (2009) in our parameter constraints.

The third fundamental advantage of using GRBs to determine the star formation rate density is that the data now goes deep into the reionization era. This makes them a rather direct probe of the star formation responsible for reionization. Importantly, we note that even though the numbers of GRBs used in the estimate are low, strong statements can still be made about the star formation rate density (Kistler et al. 2009; Yüksel et al. 2008). Of course the addition of more high redshift GRBs in the future will aid our understanding of the reionization era by lowering the statistical errors on estimation of the star formation rate density.

## 2.1 Summary of star formation rate density from high- $z$ GRBs

As discussed above, Kistler et al. (2009) have determined the star formation rate density deep into the reionization era based on the occurrence of GRBs at  $z > 6$ . We use as constraints the determination of star formation rate density based on GRBs between  $4 \lesssim z \lesssim 8.5$  from Kistler et al. (2009). In units of solar masses per year per cubic Mpc, the values used are  $\dot{\rho}_{\star, \text{obs}} = 0.06_{-0.05}^{+0.14}$  at  $z = 7.75 \pm 0.75$ ,  $\dot{\rho}_{\star, \text{obs}} = 0.1_{-0.07}^{+0.17}$  at  $z = 6.5 \pm 0.5$ ,  $\dot{\rho}_{\star, \text{obs}} = 0.07_{-0.04}^{+0.05}$  at  $z = 5.5 \pm 0.5$ , and  $\dot{\rho}_{\star, \text{obs}} = 0.13_{-0.05}^{+0.07}$  at  $z = 4.5 \pm 0.5$ . When combined with the fact that CMB constraints (Komatsu et al. 2009) place most of the reionization at  $z \sim 10$  this implies that we now have multiple constraints probing epochs during the reionization era. These data are shown in the upper right panel of Figure 1.

## 3 ADDITIONAL OBSERVATIONAL CONSTRAINTS

In this section we summarise two additional pieces of data that constrain the possible scenarios in addition to the GRB derived star formation rate density.

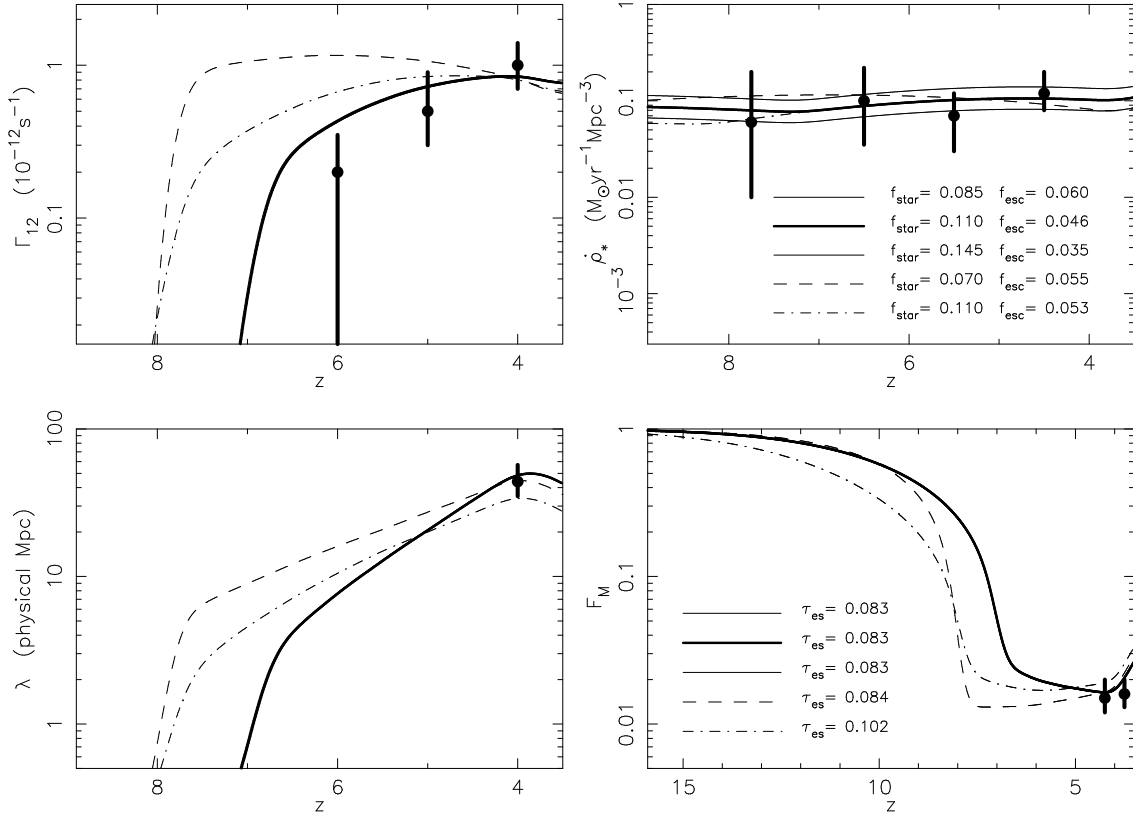


**Figure 1.** Models for the reionization of the IGM and the subsequent post-overlap evolution of the ionizing radiation field. In each panel 5 cases are shown, with line-styles corresponding to the cases in Figures 2-3. The three solid lines shown correspond to the best fit (thick line) and 1-sigma deviations for the fiducial case with  $T_{\min} = 10^4\text{K}$  and  $T_{\text{ion}} = 10^5\text{K}$  (note that these 3 cases for the fiducial model overlap in some of the panels). The dashed line shows a case with  $T_{\min} = T_{\text{ion}} = 10^4\text{K}$ . The dot-dashed line shows a case with  $T_{\min} = 10^4\text{K}$  and  $T_{\text{ion}} = 10^5\text{K}$ , but  $f_{\text{esc}} \propto (1+z)$ . The models are labeled by the values of  $f_*$ ,  $f_{\text{esc}}$  and  $\tau_{\text{es}}$ . A value of  $\Delta_c = 10$  was chosen for the critical overdensity prior to the overlap epoch. The histories shown correspond to best fit models based on constraints from  $\Gamma_{12}$  and  $\dot{\rho}_*$  at  $z > 4$ , and also  $\tau_{\text{es}}$ . *Upper Left Panel:* The ionization rate as a function of redshift. The observational points are from Bolton & Haehnelt (2007). *Upper Right Panel:* The star formation rate density as a function of redshift. The data points are from Kistler et al. (2009). *Lower Left Panel:* The mean-free-path for ionizing photons. The data point is based on Storrie-Lombardi et al. (1994). *Lower Right Panel:* The volume and mass averaged fractions of neutral gas in the universe. The observational points for the mass-fractions are from the damped Ly $\alpha$  measurements of Prochaska et al. (2005).

### 3.1 Thomson scattering optical depth for CMB photons

The measured optical depth to Thomson scattering of CMB photons measures the column density of ionized hydrogen between the observer and the surface of last scattering. The latest observed value of  $\tau_{\text{es}} = 0.084 \pm 0.016$  implies that reionization did not occur significantly beyond  $z \sim 10$  (Komatsu et al. 2009). When computing  $\tau_{\text{es}}$  from the reionization history we assume that the filling factor of singly ionized helium equals the ionized fraction of hydrogen, and that helium becomes doubly ionized at  $z = 3$  (Wyithe & Loeb 2003).

### 3.2 Ionization rate from the Ly $\alpha$ forest

Observations of the Gunn-Peterson optical depth in the high redshift Ly- $\alpha$  forest imply a very highly ionized IGM at  $z \lesssim 6$ , suggesting that reionization was complete by that time. The intensity of the ionizing background implied by the effective Ly $\alpha$  optical depth is sensitive to the details of the distribution of gas densities and temperatures,

but can be reliably modeled via numerical simulation (e.g., Bolton & Haehnelt 2007). We take values for the ionization rate at  $4 \lesssim z \lesssim 6$  from the simulations of Bolton & Haehnelt (2007), based on the observations of Fan et al. (2006). In units of  $10^{-12}\text{s}^{-1}$  the values used are  $\Gamma_{\text{obs}} = 0.2^{+0.15}_{-0.2}$  at  $z = 6$ ,  $\Gamma_{\text{obs}} = 0.5^{+0.4}_{-0.2}$  at  $z = 5$ ,  $\Gamma_{\text{obs}} = 1^{+0.4}_{-0.3}$  at  $z = 4$  respectively. These data are shown in the upper left panel of Figure 1.

## 4 SEMI-ANALYTIC MODEL FOR REIONIZATION

In this section we summarise the semi-analytic model used to calculate the reionization history of the IGM. The basis of this model is the differential between ionization and recombination rates for hydrogen in an inhomogeneous IGM. Miralda-Escudé et al. (2000) presented a model that allows the calculation of an effective recombination rate in an inhomogeneous universe by assuming a maximum overdensity ( $\Delta_c$ ) penetrated by ionizing photons within HII regions. The model assumes that reionization progresses rapidly through

islands of lower density prior to the overlap of individual cosmological ionized regions. Following the overlap epoch, the remaining regions of high density are gradually ionized. It is therefore hypothesized that at any time, regions with gas below some critical overdensity  $\Delta_i \equiv \rho_i / \langle \rho \rangle$  are highly ionized while regions of higher density are not. The fraction of mass in regions with overdensity below  $\Delta_i$ , is found from the integral

$$F_M(\Delta_i) = \int_0^{\Delta_i} d\Delta P_V(\Delta)\Delta, \quad (2)$$

where  $P_V(\Delta)$  is the volume weighted probability distribution for  $\Delta$ . Miralda-Escudé et al. (2000) quote a fitting function that provides a good fit to the volume weighted probability distribution for the baryon density in cosmological hydrodynamical simulations. In what follows, we draw primarily from the prescription of Miralda-Escudé et al. (2000) and refer the reader to the original paper for a detailed discussion of its motivations and assumptions. Wyithe & Loeb (2003) employed this prescription within a semi-analytic model of reionization. This model was extended by Srbinovsky & Wyithe (2007) and by Wyithe et al. (2008). We refer the reader to those papers for a full description.

The quantity  $Q_i$  is defined to be the volume filling factor within which all matter at densities below  $\Delta_i$  has been ionized. The reionization history is quantified by the evolution of  $Q_i$  that evolves according to the rate equation

$$\frac{dQ_i}{dz} = \frac{1}{n_0 F_M(\Delta_i)} \frac{dn_\gamma}{dz} - \left[ \alpha_B (1+z)^3 R(\Delta_i) n_0 \frac{dt}{dz} + \frac{dF_M(\Delta_c)}{dz} \right] \frac{Q_i}{F_M(\Delta_i)},$$

where  $\alpha_B$  is the case B recombination coefficient,  $n_0$  is the comoving density of hydrogen in the mean IGM, and  $R(\Delta_i)$  is the effective clumping factor of the IGM. The evolution is driven by the rate of emission of ionizing photons per co-moving volume  $dn_\gamma/dz$ . Within this formalism, the epoch of overlap is precisely defined as the time when  $Q_i$  reaches unity. Prior to the overlap epoch we must solve for both  $Q_i$  and  $F_M$  (or equivalently  $\Delta_i$ ). The relative growth of these depends on the luminosity function and spatial distribution of the sources. In this regime we assume  $\Delta_i$  to be constant with redshift before the overlap epoch and compute results for models with values of  $\Delta_i \equiv \Delta_c = 10$ .

Following overlap  $Q_i = 1$  and we describe the post-overlap evolution of the IGM by computing the evolution of the ionized mass fraction according to the equation

$$\frac{dF_M(\Delta_i)}{dz} = \frac{1}{n_0} \frac{dn_\gamma}{dz} - \alpha_B \frac{R(\Delta_i)}{a^3} n_0 \frac{dt}{dz}. \quad (3)$$

Note that in this post overlap regime the value of  $\Delta_i$  is the dependent variable describing the ionization state of the IGM and is solved for as a function of redshift.

The emission rate of ionizing photons per co-moving volume that is required to compute the reionization history can be written

$$\frac{dn_\gamma}{dz} = N_\gamma f_{\text{esc}} \frac{\dot{\rho}_\star}{m_p} \frac{dt}{dz}, \quad (4)$$

where  $N_\gamma$  is the number of ionizing photons produced per baryon incorporated into stars, and  $\dot{\rho}_\star$  is the star forma-

tion rate per unit volume. As described in the introduction, only a fraction of ionizing photons produced by stars enter the IGM. Therefore an additional factor of  $f_{\text{esc}}$  (the escape fraction) must be included when computing the ionizing emissivity of galaxies. There are expected to be large fluctuations in escape fraction with time and with viewing angle for individual galaxies. The escape fraction could also depend on galaxy mass (Gnedin et al. 2007). However what is important for studies of the overall photon budget during reionization is the total cosmic ionizing flux, rather than the ionizing flux near a particular galaxy (although of course the latter could affect statistics of Ly $\alpha$  absorption or 21cm emission from the IGM). In our model we therefore assume a single value for  $f_{\text{esc}}$ , which should be interpreted as a stellar mass averaged value over star forming galaxies.

The star formation rate per unit volume is computed based on the collapsed fraction obtained from the Press & Schechter (1974) model in halos above the minimum halo mass for star formation, together with an assumed star formation efficiency ( $f_\star$ )

$$\dot{\rho}_\star = f_\star \rho_c \Omega_B \left( (1 - Q_i) \frac{dF_{\text{col}}(M_{\text{min}})}{dt} + Q_i \frac{dF_{\text{col}}(M_{\text{ion}})}{dt} \right), \quad (5)$$

where  $\rho_c$  is the critical density and the collapsed fraction includes separate components from ionized and neutral regions of IGM. In a cold neutral IGM beyond the redshift of reionization, the collapsed fraction should be computed for halos of sufficient mass to initiate star formation. The critical virial temperature is set by the temperature ( $T_{\text{min}} \sim 10^4$  K) above which efficient atomic hydrogen cooling promotes star formation. Following the reionization of a region, the Jeans mass in the heated IGM limits accretion to halos above  $T_{\text{ion}} \sim 10^5$  K (Efstathiou 1992; Thoul & Weinberg 1996; Dijkstra et al. 2004). Thus, once  $N_\gamma$ ,  $T_{\text{min}}$  and  $T_{\text{ion}}$  are specified, the reionization model has 2 free parameters  $f_\star$  and  $f_{\text{esc}}$ .

In order to estimate the ionizing background following the end of reionization, our approach is to compute a reionization history given a particular value of  $\Delta_c$ , combined with assumed values for the efficiency of star-formation and the fraction of ionizing photons that escape from galaxies. With this history in place we then compute the evolution of the background radiation field due to these same sources. After the overlap epoch, ionizing photons will experience attenuation due to residual overdense pockets of HI gas. We use the description of Miralda-Escudé et al. (2000) to estimate the ionizing photon mean-free-path [with a reduction of the constant of proportionality by a factor of 2 following the discussion of Oh & Furlanetto (2005)], and subsequently derive the attenuation of ionizing photons. We then compute the flux at the Lyman-limit in the IGM due to sources immediate to each epoch, in addition to redshifted contributions from earlier epochs.

#### 4.1 Star formation and the production of ionizing photons

In our modeling we assume spectral energy distributions (SED) of population-II star forming galaxies using the model presented in Leitherer et al. (1999). We assume stars of 0.05 solar metallicity (the effect of metallicity is discussed in

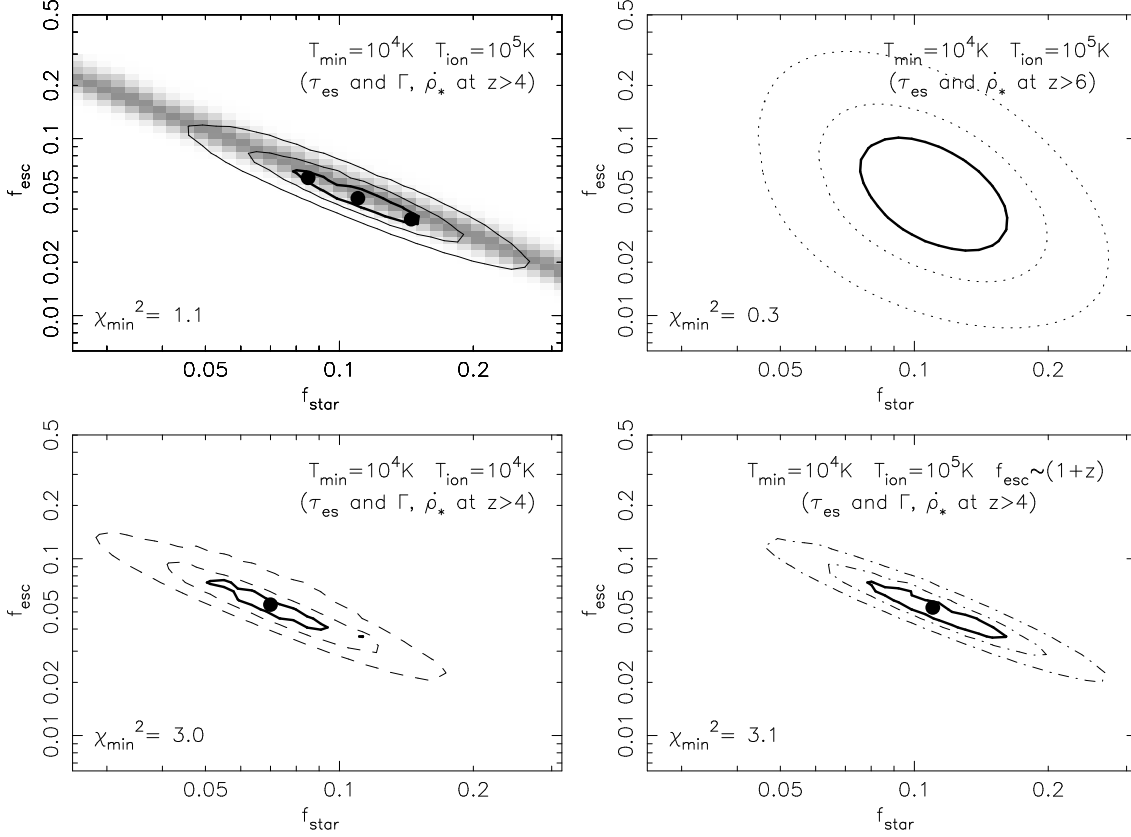


**Figure 2.** Joint constraints on the parameters  $f_*$  and  $f_{\text{esc}}$  based on observations of the star formation rate density  $\dot{\rho}_*$ , the ionization rate  $\Gamma_{12}$  and the optical depth to Thomson scattering of CMB photons  $\tau_{\text{es}}$ . *Upper Left:* The fiducial model with  $T_{\text{min}} = 10^4\text{K}$  and  $T_{\text{ion}} = 10^5\text{K}$ . Constraints on  $\Gamma_{12}$  and  $\dot{\rho}_*$  are used at  $z > 4$ . Also shown for comparison are the constraints on this model if measurements of  $\dot{\rho}_*$  are ignored, which reveals how the GRB star formation data break the degeneracy (gray shading). *Upper Right:* The fiducial model with  $T_{\text{min}} = 10^4\text{K}$  and  $T_{\text{ion}} = 10^5\text{K}$ . Constraints on  $\dot{\rho}_*$  are used at  $z > 6$ . *Lower Left:* A model with  $T_{\text{min}} = T_{\text{ion}} = 10^4\text{K}$ . Constraints on  $\Gamma_{12}$  and  $\dot{\rho}_*$  are used at  $z > 4$ . *Lower Right:* A model with  $T_{\text{min}} = 10^4\text{K}$  and  $T_{\text{ion}} = 10^5\text{K}$ , and  $f_{\text{esc}} \propto (1+z)$ . Constraints on  $\Gamma_{12}$  and  $\dot{\rho}_*$  are used at  $z > 4$ . In each case three contours are shown corresponding to differences in  $\chi^2$  relative to the best fit model of  $\Delta\chi^2 = \chi^2 - \chi_{\text{min}}^2 = 1, 2.71$  and  $6.63$ . Projections of these contours onto the axes provide the 68.3%, 90% and 99% confidence intervals on individual parameter values. The large dots show parameters of model histories presented in Figure 1.

§ 5.5), and calculate the number ( $N_\gamma$ ) of ionizing photons above the ionization threshold for hydrogen. This number is calculated for continuous star-formation, and the low solar metallicity is reasonable at high redshift. The mass functions each have lower and upper limits of  $0.1M_\odot$  and  $120M_\odot$  respectively. Taking the functional form  $dn/dM \propto M^{-\alpha}$ , our fiducial model has a Salpeter IMF with  $\alpha = 2.35$  (we also discuss other choices for the IMF in § 5.5). With these choices we find  $N_\gamma = 4648$  in our fiducial model.

## 5 CONSTRAINTS ON MODELS OF THE REIONIZATION HISTORY

In this section we confront our model for reionization with the three pieces of data described in earlier sections in order to constrain the possible scenarios.

### 5.1 Parameter constraints

From the above observations we constrain the possible parameterizations of our model for the reionization history. In addition to hypothesised parameters  $\Delta_c$ ,  $T_{\text{min}}$  and  $T_{\text{ion}}$ , our

reionization model has two free parameters,  $f_*$  and  $f_{\text{esc}}$ , for combinations of which we compute the reionization history, and calculate the  $\chi^2$  of the model as

$$\begin{aligned} \chi^2(f_*, f_{\text{esc}}) = & \sum_{i=0}^{N_{\Gamma, \text{obs}}} \left( \frac{\log \Gamma(f_*, f_{\text{esc}}) - \log \Gamma_{\text{obs}}}{\sigma_\Gamma} \right)^2 \\ & + \sum_{i=0}^{N_{\dot{\rho}_*, \text{obs}}} \left( \frac{\log \dot{\rho}_*(f_*, f_{\text{esc}}) - \log \dot{\rho}_{*, \text{obs}}}{\sigma_\rho} \right)^2 \\ & + \left( \frac{\tau_{\text{es}}(f_*, f_{\text{esc}}) - \tau_{\text{es, obs}}}{\sigma_\tau} \right)^2. \end{aligned} \quad (6)$$

Here  $\Gamma_{\text{obs}}$  and  $\dot{\rho}_*$  are the observed ionization rates and star formation rate densities measured at a number of redshifts, with uncertainty  $\sigma_\Gamma(r_i)$  and  $\sigma_\rho$  (in dex), and  $\tau_{\text{es, obs}}$  is the observed optical depth to Thomson scattering of CMB photons with uncertainty  $\sigma_\tau$  (in dex). We note that the error bars on the observational estimates are not symmetric.

## 5.2 Constraints on the escape fraction in the fiducial model

In the upper left panel of Figure 2, we present constraints on the parameters  $f_*$  and  $f_{\text{esc}}$  assuming our fiducial model with  $T_{\text{min}} = 10^4\text{K}$ , and  $T_{\text{ion}} = 10^5\text{K}$ . As a first illustration we have included the available constraints on  $\tau_{\text{es}}$  as well as on  $\Gamma$ , but have neglected  $\dot{\rho}_*$  in order to highlight the importance of its inclusion with the latter examples. The allowed region in this case is shown by the gray shading. The ionizing background radiation, and the duration of the reionization epoch as measured by  $\tau_{\text{es}}$  constrain the combination  $f_{\text{star}} f_{\text{esc}}$  (Barkana & Loeb 2001; Srinovsky & Wyithe 2008). This degeneracy can be clearly seen in Figure 2. The dark solid contours that are over plotted in the upper left panel of Figure 2 show the corresponding constraints following addition of measurements of  $\dot{\rho}_*$  from  $z > 4$ . The star formation rate breaks this degeneracy, since the star formation rate density predicted by the model is not directly dependent<sup>1</sup> on  $f_{\text{esc}}$ . As a result,  $f_*$  and  $f_{\text{esc}}$  can be separately constrained yielding values of  $0.085 \lesssim f_* \lesssim 0.145$  and  $0.035 \lesssim f_{\text{esc}} \lesssim 0.060$  for the fiducial model. The best fit model has the parameter combination  $(f_*, f_{\text{esc}}) = (0.110, 0.046)$ , with a value of  $\chi_{\text{min}}^2 = 1.1$ . This value is total rather than per degree-of-freedom, and is surprisingly low given a 2 parameter fit and 8 data points which may indicate that the error bars are overestimated. However we note that the values for 3 additional free parameters have been chosen in this model ( $T_{\text{min}}$ ,  $T_{\text{ion}}$  and  $\Delta_c$ ). Different values for these are assumed below, leading to larger  $\chi^2$  values.

In Figure 1 we show models (solid lines) corresponding to the best fit,  $(f_*, f_{\text{esc}}) = (0.110, 0.046)$ , as well as models near the edge of the 1-sigma contour,  $(f_*, f_{\text{esc}}) = (0.085, 0.060)$  and  $(f_*, f_{\text{esc}}) = (0.145, 0.035)$ . The locations of these models in the  $f_*$ - $f_{\text{esc}}$  plane are shown by dots in Figure 2. In the upper left and upper right panels of Figure 1 we show the evolution of the ionization rate and star formation rate density respectively. In the lower left and lower right panels we show the evolution of the ionizing photon mean-free-path and mass averaged neutral fraction that are also predicted by the model. Note that the quantities other than star formation rate density are degenerate for these parameter combinations. The data points for mean-free-path are based on Storrie-Lombardi et al. (1994). The observational points for the mass-fractions are from the damped Ly $\alpha$  measurements of Prochaska et al. (2005), and therefore represent lower limits on the total HI content of the IGM. In both cases the curves show excellent agreement with these quantities, even though they were not included as part of the parameter fit. The values of  $\tau_{\text{es}}$  for these models are listed in the lower right panel. The universe is predicted to be 50% ionized at  $z \sim 9.5$ .

We note that the observed mean-free-path is found from the number density of Ly-limit systems and is independent of the Ly $\alpha$  forest absorption derived quantities of ionization rate and volume averaged neutral fraction, as well as being independent of the HI mass-density measurements. Our simple model therefore simultaneously reproduces the evo-

lution of four independent measured quantities, as well as the optical depth to electron scattering of CMB photons.

Despite this success, the accuracy of estimates for the ionization rates predicted by the model could be questioned, primarily because of the sensitivity of the calculation of the mean-free-path to the probability distribution for  $\Delta$ . To test the sensitivity of our conclusion regarding the value of escape fraction to the use of  $\Gamma$  as a constraint, we therefore investigate the constraints available when only the observations of  $\dot{\rho}_*$  are used in addition to  $\tau_{\text{es}}$ . The constraints are shown in the upper right panel of Figure 2. In this case the best fit model has the same parameter combination  $(f_*, f_{\text{esc}}) = (0.110, 0.046)$ , with a lower value of  $\chi_{\text{min}}^2 = 0.3$ . Thus removing the  $\Gamma$  points loosens the constraints on  $f_*$  and  $f_{\text{esc}}$  but does not alter the best fit values. We find values of  $0.075 \lesssim f_* \lesssim 0.16$  and  $0.025 \lesssim f_{\text{esc}} \lesssim 0.10$  in this case.

In Figure 3 we show the marginalised distribution of  $f_{\text{esc}}$ . The line styles are consistent with those chosen for the corresponding contours of  $\chi^2$  in Figure 2. In constructing the marginalised likelihoods we have assumed prior probability distributions for  $f_*$  and  $f_{\text{esc}}$  that are flat in the logarithm, i.e.,  $dP_{\text{prior}}/d \log f_* \propto 1$  and  $dP_{\text{prior}}/d \log f_{\text{esc}} \propto 1$ .

## 5.3 Effect of radiative feedback on low mass galaxies

There is some theoretical uncertainty surrounding the strength of radiation feedback on the formation of low mass galaxies (Dijkstra et al. 2004; Mesinger & Dijkstra 2008). We therefore repeat our constraints on  $f_*$  and  $f_{\text{esc}}$  using a modification of the fiducial model with no radiative feedback, i.e.,  $T_{\text{min}} = T_{\text{ion}} = 10^4\text{K}$ . The constraints based on this model are shown in the lower left panel of Figure 2. The best fit modified model has the parameter combination  $(f_*, f_{\text{esc}}) = (0.070, 0.055)$ , with a value of  $\chi_{\text{min}}^2 = 3.0$  (this model is therefore disfavoured by the data relative to the fiducial case). As reionization progresses, more gas is allowed to accrete into galaxies in this case than in the fiducial model. As a result the star formation efficiency required to produce the observed star formation rate density is reduced. We find values of  $0.05 \lesssim f_* \lesssim 0.095$  and  $0.04 \lesssim f_{\text{esc}} \lesssim 0.08$  for this model. Thus the details of the stellar mass accretion rate influence the inferred star formation efficiency, but only weakly effect the inferred escape fraction of ionizing photons.

Figure 3 shows the corresponding marginalised distribution for escape fraction (dashed line). As noted above, the removal of radiative feedback from the model has little effect on the derived escape fraction distribution. On the other hand the reionization history is quite different in this case. The dashed lines in Figure 1 show the best fit model in this case  $(f_*, f_{\text{esc}}) = (0.07, 0.055)$ . The lower value of  $f_*$  means that reionization gets underway later. However despite this reionization is finished earlier, with an associated rise in the ionizing background at higher redshifts in this case than in the fiducial model. This rapid rise occurs because reionization is assumed not to be self limiting in this case and so is completed by low mass galaxies.

<sup>1</sup> There is an indirect dependence of star formation rate density on  $f_{\text{esc}}$  because the star formation rate depends on the fraction of universe ionized at a particular time.

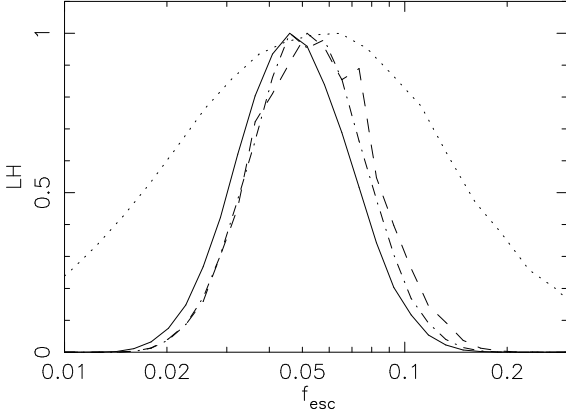


**Figure 3.** Constraints on the parameter  $f_{\text{esc}}$  corresponding to marginalisation of the joint distributions in Figure 2 (the line styles are the same for the joint and marginalised distributions in these figures). *Solid line:* The fiducial model with  $T_{\text{min}} = 10^4\text{K}$  and  $T_{\text{ion}} = 10^5\text{K}$ . Constraints on  $\Gamma_{12}$  and  $\dot{\rho}_*$  are used at  $z > 4$ . *Dotted line:* Constraints on the fiducial model without inclusion of  $\Gamma_{12}$ . *Dashed Line:* A model with  $T_{\text{min}} = T_{\text{ion}} = 10^4\text{K}$ . Constraints on  $\Gamma_{12}$  and  $\dot{\rho}_*$  are used at  $z > 4$ . *Dot-Dashed Line:* A model with  $T_{\text{min}} = 10^4\text{K}$  and  $T_{\text{ion}} = 10^5\text{K}$ , and  $f_{\text{esc}} \propto (1+z)$ . Constraints on  $\Gamma_{12}$  and  $\dot{\rho}_*$  are used at  $z > 4$ .

#### 5.4 Evolving escape fraction

Our modeling so far has assumed an escape fraction that is constant with redshift. To test the impact of this assumption on the value of  $f_{\text{esc}}$  we therefore consider a case where our fiducial model is modified so that  $f_{\text{esc}}(z) = f_{\text{esc}}(1+z)/7$ , and constrain the value of  $f_{\text{esc}}$  at  $z = 6$ . The results are shown in the lower right panel of Figure 2. In this case we find values which are very similar to the fiducial case,  $0.085 \lesssim f_* \lesssim 0.145$  and  $0.035 \lesssim f_{\text{esc}} \lesssim 0.06$  for this model. The best fit model has the parameter combination  $(f_*, f_{\text{esc}}) = (0.11, 0.053)$ , with a value of  $\chi_{\text{min}}^2 = 3.1$  (this model is therefore also disfavoured relative to the fiducial case).

Figure 3 shows the corresponding marginalised distribution for escape fraction (dot-dashed line). The evolution of escape fraction is degenerate with evolution in the mass accretion rate of galaxies, and so as in the previous example has little effect on the derived escape fraction distribution. The dot-dashed lines in Figure 1 show the best fit model in this case  $(f_*, f_{\text{esc}}) = (0.11, 0.053)$ . The reionization history is again quite different from the fiducial model. The larger value of  $f_{\text{esc}}$  towards high redshift results in an earlier reionization and a higher  $\tau_{\text{es}}$ .

#### 5.5 Uncertainty in the choice of IMF

Both the number of ionizing photons produced per star as well as the star formation rate density inferred from the number of GRBs observed during the reionization era depend on the IMF assumed. The former dependence arises because more massive stars are hotter and therefore emit a larger fraction of their energy at frequencies above the ionization threshold for hydrogen. Regarding the latter dependence, we note that the relation between the GRB rate and the star formation rate density is calibrated at redshifts below  $z \sim 4$  where they can each be separately determined

(Kistler et al. 2009). Most of the star formation rate indicators (e.g.,  $\text{H}\alpha$ ) probe only massive stars, and hence a correction involving an IMF is required. However, what is important for the present analysis is the number of ionizing photons implied by the observed number of high redshift GRBs, i.e., relating one quantity depending just on massive stars to another. With respect to this quantity the dependencies on IMF mentioned tend to cancel, because a more top-heavy IMF leads to increases in both the GRB rate and the number of ionizing photons produced. We note here that within the context of studies of the star formation history, *top-heavy* can really be interpreted to mean *bottom-light*. This is because one measures the light (or the birth/death rate) from the massive stars and infers the contribution to stellar mass from lower masses. In other words the analysis is normalized by the high-mass end of the IMF. This situation would be reversed if one were looking at the integrated stellar mass, which is dominated by low-mass stars.

To assess the systematic error in determination of the escape fraction introduced by the choice of IMF we consider a range of initial mass functions (IMF), as summarised in Table 1. As in our fiducial case, we assume stars of 0.05 solar metallicity, and present the number of ionizing photons above the ionization threshold for hydrogen. This number is again calculated with mass functions that have lower and upper limits of  $0.1M_{\odot}$  and  $120M_{\odot}$  respectively. We consider two cases with turnover in the mass function below  $0.5M_{\odot}$  (with an index in that mass range of  $\alpha = 1.5$ ). These cases have high mass indexes of  $\alpha = 2.35$  (labeled Salpeter A) and  $\alpha = 2.15$  (Baldry & Glazebrook 2003, labeled BG) respectively. The Salpeter A and BG IMFs were identified by Hopkins & Beacom (2006) as providing reasonable bounds on the normalisation of the cosmic star formation history. We also consider the case of a top-heavy mass function having a single index of  $\alpha = 1.95$  across the entire mass range. The values for  $N_{\gamma}$  are listed in Table 1, demonstrating that more top-heavy mass functions produce a larger fraction of their energy as photons above the ionization threshold. The ratio relative to the value  $N_{\text{sal}} = 4648$  for a Salpeter mass function is also presented in the second last column for ease of comparison.

In the 4th column of Table 1 we show the fraction of the star formation inferred assuming a Salpeter IMF that would have been derived in Kistler et al. (2009) if a different IMF had been used instead. Where a more top-heavy IMF is assumed, the star-formation rate density implied by the observed GRBs is reduced by this factor relative to our fiducial model. Since a change in the assumed IMF leads to a change in the inferred star formation rate density, it also leads to a proportional change in the derived star formation efficiency. Thus for each IMF listed the value of  $\dot{\rho}_*/\dot{\rho}_{\text{sal}}$  represents the size of the systematic uncertainty in constraints on  $f_*$ .

The change in IMF also leads to a change in  $N_{\gamma}$ , and the escape fraction required to reproduce the observables of reionization is therefore proportional to  $(\dot{\rho}_* N_{\gamma})^{-1}$ . In the final column we list the quantity

$$f_{\text{IMF}} \equiv \dot{\rho}_*/\dot{\rho}_{\text{sal}} \times N_{\gamma}/N_{\text{sal}}, \quad (7)$$

which gives the ratio of ionizing photons to GRBs, relative to the Salpeter IMF. The range in values of  $f_{\text{IMF}}$  provides an estimate of the systematic uncertainty in the derived escape

**Table 1.** Summary of IMFs used in this work.

IMF	$\alpha_{\text{low}}$	$\alpha$	$\dot{\rho}_*/\dot{\rho}_{\text{sal}}$	$N_\gamma$	$N_\gamma/N_{\text{sal}}$	$f_{\text{IMF}}$
Salpeter	-	2.35	1	4648	1	1.00
Salpeter A	1.5	2.35	0.77	6034	1.30	1.00
BG03	1.5	2.15	0.50	11139	2.39	1.20
Top-Heavy	-	1.95	0.37	17553	2.75	1.39

fraction owing to the choice of IMF. As expected, the net effect on the reionization considerations caused by choosing a different IMF is quite modest. It is possible that the IMF is evolving with look back time. In this case, by extension of the above arguments our estimate of the escape fraction would sustain only a small systematic uncertainty. Importantly, we find that for metal enriched stellar populations, the choice of IMF contributes a systematic uncertainty on the derived escape fraction of only  $\sim 0.1$  dex.

Finally, we note that the assumed metallicity can have an effect on both the calibration of star formation rate density, and on the value of  $N_\gamma$  computed for a particular IMF. Calibrations of star formation rate density are performed locally and so refer to solar metallicity. On the other hand we have assumed a metallicity of 1/20th solar in computing the reionization history, as may be more appropriate at high redshift. The Salpeter IMF with solar metallicity yields  $N_\gamma = 3328$  ionizing photons per baryon, a factor of 1.4 times smaller than in our fiducial model. This metallicity uncertainty corresponds to an additional  $\sim 0.1$  dex uncertainty on  $f_{\text{esc}}$ . It may be possible to remove this metallicity uncertainty in the determination of  $f_{\text{esc}}$  by noting that many star formation rate indicators (e.g.,  $\text{H}\alpha$ ) are proportional to the ionizing flux, so that the higher number of ionizing photons for low metallicity stars is offset by a smaller inferred star-formation rate. We have not pursued this in the current work. We conservatively estimate that accounting for the uncertainties in IMF and metallicity leads to  $\sim 0.2$  dex of systematic uncertainty in the determination of  $f_{\text{esc}}$  from our analysis.

### 5.6 Reionization by X-rays

Our analysis has thus far assumed that reionization is entirely due to high mass stars. However in addition to UV photons from the first galaxies and quasars, it has been suggested that a background of X-ray photons at very high redshift may be important (e.g., Ricotti & Ostriker 2004). Indeed, several authors have proposed an initial phase of preheating and partial ionization of the IGM by X-rays, resulting primarily from black hole accretion (e.g., Shull & van Steenberg 1985; Venkatesan et al. 2001; Ricotti & Ostriker 2004). An X-ray background could also have originated from X-ray binaries and supernova remnants. In difference to UV photons, X-rays ionize hydrogen both directly and through secondary ionizations by photoelectrons from ionized helium, with the latter dominating so that many hydrogen atoms can be ionized by a single X-ray photon. As reionization proceeds, however, the proportion of each X-rays energy that is deposited into the IGM as heat, increases. In particular, for ionization fractions

$\gtrsim 10\%$ , ionization by secondary electrons becomes inefficient (Ricotti & Ostriker 2004). As a result, X-ray ionization is self regulating at the level of  $\sim 10 - 20\%$ . Modeling the possible contribution of X-rays to reionization is beyond the scope of this paper. However the self-regulation implies that neglect of X-rays would lead to an overestimation of  $f_{\text{esc}}$  by this factor at most, and we therefore estimate a systematic component of uncertainty owing to the unknown X-ray contribution to reionization of  $\sim 0.05$  dex.

### 5.7 Numerical constraints on the escape fraction

Our fiducial model constrains the escape fraction to have a value  $\log f_{\text{esc}} = -1.35 \pm 0.15$  (68%). Of the systematic errors discussed the largest arise due to uncertainty in the IMF and in the metallicity of the star forming populations responsible for reionization. We estimate that each of these contribute  $\sim 0.1$  dex of systematic uncertainty. Thus in summary of our analysis we find  $\log f_{\text{esc}} = (-1.35 \pm 0.15) \pm 0.2$ .

## 6 SUMMARY

The fraction of ionizing photons that escape their host galaxy and so are able to ionize hydrogen in the intergalactic medium (IGM) is a critical parameter in studies of the reionization era and early galaxy formation. Indeed as can be seen directly from equation (1), the amount of star formation required to reionize the Universe is inversely proportional to the escape fraction. Determination of the expected value for the escape fraction is problematic for individual galaxies. Observationally, very deep spectra must be obtained to overcome absorption in the IGM and detect photons that escape the host galaxy at energies beyond the Ly limit. Theoretical calculation of escape fraction is difficult owing to the large dynamic range and complex gas and star formation physics that must be modeled to resolve the clumpy ISM.

Many studies of the reionization history have compared theoretical models to the electron scattering optical depth of CMB photons, and the ionization rate from the Ly $\alpha$  forest at the end of the overlap era. These studies are subject to degeneracies between the escape fraction of ionizing photons, and the efficiency with which high redshift galaxies turn mass into stars (e.g., Wyithe & Loeb 2003; Haiman & Holder 2003; Cen 2003; Choudhury & Ferrara 2005; Shull & Venkatesan 2008). While upper limits have previously been obtained for surveys of high redshift star forming galaxies (Bouwens et al. 2008), the recent determination of the star formation rate density during the reionization era from the most distant Gamma Ray Bursts discovered provides the first method for directly measuring the star formation rate density during the reionization era. With respect to calculating the escape fraction, this method has the advantages over estimates of star formation rate from the galaxy luminosity function that it directly observes the total star formation rate (i.e., no correction for a galaxy flux limit), and is well calibrated at lower redshift (Kistler et al. 2009).

In this paper we have used this first determination of the star formation rate density at  $z > 6$  to break the degeneracy between star formation efficiency and escape fraction.

Our analysis employed a semi-analytic model for reionization that we confronted with three complementary sets of observations, *i*) the electron scattering optical depth of CMB photons, *ii*) the ionization rate from the Ly $\alpha$  forest at the end of the overlap era and *iii*) The star formation rate density out to  $z = 8.5$ . By constraining the model parameters with these observations we show that the escape fraction of ionizing photons from high redshift galaxies is  $f_{\text{esc}} \sim 5\%$ . For our fiducial model we find  $\log f_{\text{esc}} = -1.35 \pm 0.15$

Importantly, this value is stable against a range of systematic uncertainties in the modeling, including the implementation of radiative feedback and the choice of IMF. In agreement with previous studies we find that the mass assembly history of galaxies was important for the reionization history, and impacts on the inferred value of star formation efficiency. However, the value of escape fraction inferred is not sensitive to the details of the mass assembly. We also investigated an evolving escape fraction, finding that this did not strongly influence the value of escape fraction inferred for galaxies at  $z = 6$ . Our modelling does make the assumption that UV photons produced by stars dominate the reionization process. A possible contribution of X-rays to reionization (Ricotti & Ostriker 2004) complicates this interpretation, and implies that our escape fraction could be overestimated by a factor up to 1.1 – 1.2. Both the number of ionizing photons and the number of GRBs per unit star formation are sensitive to the IMF. The dependencies on IMF tend to cancel in our analysis, however we considered a range of possibilities. We estimate an uncertainty of  $\sim 0.1$  dex in  $f_{\text{esc}}$  owing to the unknown shape of the IMF, and another  $\sim 0.1$  dex owing to the unknown metallicity of the galaxies responsible for reionization. Including these uncertainties we express our estimate of escape fraction as  $\log f_{\text{esc}} = (-1.35 \pm 0.15) \pm 0.2$ . Our analysis assumed that the escape fraction is independent of galaxy mass. Previous work has suggested that lower mass galaxies have smaller escape fractions (Gnedin et al. 2007). In this scenario our escape fraction should be considered as a stellar mass weighted average over star forming galaxies.

Our simple semi-analytic model is able to provide a statistically acceptable fit to the available observations under a range of assumptions. This implies that models of the reionization history are under constrained [although more variables could potentially be used as constraints Choudhury & Ferrara (2005, 2006)]. In the near future 21cm observations of neutral IGM during the reionization era will provide a powerful new probe. Lidz et al. (2008) have shown that the first generation of low frequency telescopes will be able to measure the neutral fraction accurately during epochs when the universe is  $\sim 50\%$  ionized. The example reionization histories presented in this and other papers illustrate that this will provide important discriminates among possible reionization histories. With respect to the escape fraction, such measurements in combination with the evolution in star formation rate density will allow for the evolution in addition to the value to be measured.

## ACKNOWLEDGEMENTS

This work was supported in part by the Australian Research Council (JSBW and AMH). MDK and JFB were supported

by NSF CAREER Grant PHY-0547102 (to JFB) and HY by DOE Grant DE-FG02-91ER40626.

## REFERENCES

- Baldry I. K., Glazebrook K., 2003, ApJ, 593, 258  
 Barkana R., Loeb A., 2001, ApJS, 349, 125  
 Bolton J. S., Haehnelt M. G., 2007, MNRAS, p. 957  
 Bouwens R. J., Illingworth G. D., Franx M., Ford H., 2008, ApJ, 686, 230  
 Cen R., 2003, ApJL, 591, L5  
 Choudhury T. R., Ferrara A., 2005, MNRAS, 361, 577  
 Choudhury T. R., Ferrara A., 2006, MNRAS, 371, L55  
 Ciardi B., Ferrara A., 2005, Space Science Reviews, 116, 625  
 Deharveng J.-M., Buat V., Le Brun V., Milliard B., Kunth D., Shull J. M., Gry C., 2001, Astron. and Astroph., 375, 805  
 Dijkstra M., Haiman Z., Rees M. J., Weinberg D. H., 2004, ApJ, 601, 666  
 Efstathiou G., 1992, MNRAS, 256, 43  
 Fan X., Narayanan V. K., Strauss M. A., White R. L., Becker R. H., Pentericci L., Rix H. W., 2002, AJ, 123, 1247  
 Fan X., Strauss M. A., Becker R. H., White R. L., Gunn J. E., Knapp G. R., Richards G. T., Schneider D. P., Brinkmann J., Fukugita M., 2006, AJ, 132, 117  
 Faucher-Giguère C.-A., Lidz A., Hernquist L., Zaldarriaga M., 2008, ApJ, 688, 85  
 Fernández-Soto A., Lanzetta K. M., Chen H.-W., 2003, MNRAS, 342, 1215  
 Fruchter A. S., Levan A. J., Strolger L., Vreeswijk P. M., Thorsett S. E., Bersier D., Burud I., Castro Cerón J. M., et al. 2006, *Nature*, 441, 463  
 Fujita A., Martin C. L., Mac Low M.-M., Abel T., 2003, ApJ, 599, 50  
 Fynbo J. P. U., Jakobsson P., Prochaska J. X., Malesani D., Ledoux C., de Ugarte Postigo A., Nardini M., Vreeswijk P. M., et al. 2009, ArXiv e-prints, arXiv:0907.3449  
 Gnedin N. Y., Kravtsov A. V., Chen H.-W., 2007, ArXiv e-prints, astro-ph/0707.0879  
 Haiman Z., Holder G. P., 2003, ApJ, 595, 1  
 Heckman T. M., Sembach K. R., Meurer G. R., Leitherer C., Calzetti D., Martin C. L., 2001, ApJ, 558, 56  
 Hopkins A. M., Beacom J. F., 2006, ApJ, 651, 142  
 Inoue A. K., Iwata I., Deharveng J.-M., 2006, MNRAS, 371, L1  
 Kistler M. D., Yuksel H., Beacom J. F., Hopkins A. M., Wyithe J. S. B., 2009, ArXiv e-prints, astro-ph/0906.0590  
 Komatsu E., Dunkley J., Nolta M. R., Bennett C. L., Gold B., Hinshaw G., Jarosik N., Larson D., Limon M., Page L., Spergel D. N., Halpern M., Hill R. S., Kogut A., Meyer S. S., Tucker G. S., Weiland J. L., Wollack E., Wright E. L., 2009, ApJS, 180, 330  
 Leitherer C., Ferguson H. C., Heckman T. M., Lowenthal J. D., 1995, ApJL, 454, L19  
 Leitherer C., Schaerer D., Goldader J. D., Delgado R. M. G., Robert C., Kune D. F., de Mello D. F., Devost D., Heckman T. M., 1999, ApJS, 123, 3  
 Lidz A., Zahn O., McQuinn M., Zaldarriaga M., Hernquist L., 2008, ApJ, 680, 962

- Lien A., Fields B. D., 2009, *Journal of Cosmology and Astro-Particle Physics*, 1, 47
- Madau P., Haardt F., Rees M. J., 1999, *ApJ*, 514, 648
- Mesinger A., Dijkstra M., 2008, *MNRAS*, 390, 1071
- Miralda-Escudé J., Haehnelt M., Rees M. J., 2000, *ApJ*, 530, 1
- Oh S. P., Furlanetto S. R., 2005, *ApJL*, 620, L9
- Press W. H., Schechter P., 1974, *ApJ*, 187, 425
- Prochaska J. X., Herbert-Fort S., Wolfe A. M., 2005, *ApJ*, 635, 123
- Razoumov A. O., Sommer-Larsen J., 2006, *ApJL*, 651, L89
- Ricotti M., Ostriker J. P., 2004, *MNRAS*, 352, 547
- Salvaterra R., Della Valle M., Campana S., Chincarini G., Covino S., D’Avanzo P., Fernandez-Soto A., Guidorzi C., et al. 2009, *ArXiv e-prints astro-ph/0906.1578*
- Shapley A. E., Steidel C. C., Pettini M., Adelberger K. L., Erb D. K., 2006, *ApJ*, 651, 688
- Shull J. M., van Steenberg M. E., 1985, *ApJ*, 298, 268
- Shull J. M., Venkatesan A., 2008, *ApJ*, 685, 1
- Siana B., Teplitz H. I., Colbert J., Ferguson H. C., Dickinson M., Brown T. M., Conselice C. J., de Mello D. F., Gardner J. P., Giavalisco M., Menanteau F., 2007, *ApJ*, 668, 62
- Srbinovsky J., Wyithe S., 2008, *ArXiv e-prints astro-ph/0807.4782*
- Srbinovsky J. A., Wyithe J. S. B., 2007, *MNRAS*, 374, 627
- Stanek K. Z., Gnedin O. Y., Beacom J. F., Gould A. P., Johnson J. A., Kollmeier J. A., Modjaz M., Pinsonneault M. H., Pogge R., Weinberg D. H., 2006, *Acta Astronomica*, 56, 333
- Steidel C. C., Pettini M., Adelberger K. L., 2001, *ApJ*, 546, 665
- Storrie-Lombardi L. J., McMahon R. G., Irwin M. J., Hazard C., 1994, *ApJL*, 427, L13
- Tanvir N. R., Fox D. B., Levan A. J., Berger E., Wiersema K., Fynbo J. P. U., Cucchiara A., Kruehler T., et al. 2009, *ArXiv e-prints astro-ph/0906.1577*
- Thoul A. A., Weinberg D. H., 1996, *ApJ*, 465, 608
- Venkatesan A., Giroux M. L., Shull J. M., 2001, *ApJ*, 563, 1
- Wood K., Loeb A., 2000, *ApJ*, 545, 86
- Wyithe J. S. B., Bolton J. S., Haehnelt M. G., 2008, *MNRAS*, 383, 691
- Wyithe J. S. B., Loeb A., 2003, *ApJ*, 586, 693
- Yüksel H., Kistler M. D., Beacom J. F., Hopkins A. M., 2008, *ApJL*, 683, L5